Concentration Dependence of Self-Assembled Monolayer Island Nucleation and Growth

Ivo Doudevski† and Daniel K. Schwartz*,‡

Contribution from the Department of Chemistry, Tulane University, New Orleans, Louisiana 70118

Received December 18, 2000. Revised Manuscript Received May 8, 2001

Abstract: We have observed the formation process of octadecylphosphonic acid self-assembled monolayers on mica in situ, at the liquid/solid interface, using atomic force microscopy. The submonolayer island nucleation rate was found to depend on the concentration of the deposition solution, which affects the deposition rate of adsorbate molecules on the substrate. The power-law dependence of the submonolayer island density on the solution concentration was consistent with the interpretation that the minimum size of a stable island is two molecules. Four distinct regimes of growth were found: a low-coverage nucleation regime, an intermediate coverage regime, an aggregation regime in which the island density remained constant, and a coalescence regime. The island density kinetics in the first two regimes were compared with the predictions of a kinetic theory of 2D cluster growth typically used to describe vapor phase molecular beam epitaxy at low temperatures.

Introduction

Self-assembled monolayers (SAMs) form as a result of spontaneous adsorption and organization of adsorbate molecules on a solid surface upon exposure to dilute solution.[1,2] One end of the adsorbate molecule (the headgroup) is designed to have a specific attractive interaction with the substrate. In recent years SAMs have attracted significant attention due to their technological promise in areas that involve surface modification and patterning such as nonlinear optics, chemical sensors, etc. These applications typically rely on a well-ordered film involving close-packed molecules with a relatively uniform molecular orientation and conformation. Experimental evidence suggests that this final film structure generally forms via a stepwise process, where two-dimensional (2D) clusters ("islands") of close-packed, approximately vertically orientated molecules, nucleate, grow, and coalesce from within a less-dense surface phase.[3−29]

The initial stage of growth involves the deposition of isolated adsorbate molecules; this can be considered a 2D "vapor" phase or, perhaps more accurately, a dilute 2D solution since surface sites between adsorbate molecules are undoubtedly filled by solvent molecules. From this point, two general classes of growth mechanism have been observed. For alkylsilanes[3−11,18,19] or alkylphosphonic acids,[12−16] under appropriate conditions, close-packed islands of the final 2D "solid" phase were found to nucleate and grow directly from the 2D vapor phase. For thiols,[22−29] alkyltrimethylammonium bromide on mica,[17] or silanes/phosphonic acids under different conditions,[5−10,16] the incomplete monolayer passes from the 2D vapor into an intermediate-density phase before nucleation and growth of solid-phase islands begin. This intermediate phase may involve conformationally disordered molecules[5−7,16,17] or it may be an ordered phase in which molecules lie flat on the surface.[22−29] For silanes on silicon oxide[5−7,20] or phosphonic acids on sapphire,[16] a distinct transition from the former growth mech-

* To whom correspondence should be addressed.
† Current address: Department of Chemical Engineering, University of California, Santa Barbara, CA 93106.
‡ Current address: Department of Chemical Engineering, University of Colorado, Boulder, CO 80309.

(1) Ulman, A. *Chem. Rev.* **1996**, *96*, 1533.
(2) Poirier, G. E. *Chem. Rev.* **1997**, *97*, 1117.
(3) Schwartz, D. K.; Steinberg, S.; Israelachvili, J.; Zasadzinski, J. A. N. *Phys. Rev. Lett.* **1992**, *69*, 3354.
(4) Bierbaum, K.; Grunze, M.; Baski, A. A.; Chi, L. F.; Schrepp, W.; Fuchs, H. *Langmuir* **1995**, *11*, 2143.
(5) Carraro, C.; Yauw, O. W.; Sung, M. M.; Maboudian, R. *J. Phys. Chem. B* **1998**, *102*, 4441.
(6) Goldmann, M.; Davidovits, J. V.; Silberzan, P. *Thin Solid Films* **1998**, *329*, 166.
(7) Sung, M. M.; Carraro, C.; Yauw, O. W.; Kim, Y.; Maboudian, R. *J. Phys. Chem. B* **2000**, *104*, 1556.
(8) Vallant, T.; Brunner, H.; Mayer, U.; Hoffmann, H.; Leitner, T.; Resch, R.; Friedbacher, G. *J. Phys. Chem. B* **1998**, *102*, 7190.
(9) Vallant, T.; Kattner, J.; Brunner, H.; Mayer, U.; Hoffmann, H. *Langmuir* **1999**, *15*, 5339.
(10) Brunner, H.; Vallant, T.; Mayer, U.; Hoffmann, H.; *Langmuir* **1999**, *15*, 1899.
(11) Resch, R.; Grasserbauer, M.; Friedbacher, G.; Vallant, T. Brunner, H.; Mayer, U.; Hoffmann, H. *Appl. Surf. Sci.* **1999**, *140*, 168.
(12) Woodward, J. T.; Schwartz, D. K. *J. Am. Chem. Soc.* **1996**, *118*, 7861.
(13) Woodward, J. T.; Doudevski, I.; Sikes, H. D.; Schwartz, D. K. *J. Phys. Chem. B* **1997**, *101*, 7535.
(14) Doudevski, I.; Hayes, W. A.; Schwartz, D. K. *Phys. Rev. Lett.* **1998**, *81*, 4927.
(15) Doudevski, I.; Schwartz, D. K. *Phys. Rev. B* **1999**, *60*, 14.
(16) Messerschmidt, C.; Schwartz, D. K. *Langmuir* **2001**, *17*, 462.
(17) Hayes, W. A.; Schwartz, D. K. *Langmuir* **1998**, *14*, 5913.
(18) Richter, A. G.; Durbin, M. K.; Yu, C.-J.; Dutta, P. *Langmuir* **1998**, *14*, 5980.
(19) Richter, A. G.; Yu, C. J.; Datta, A.; Kmetko, J.; Dutta, P. *Phys. Rev. E* **2000**, *61*, 607.
(20) Parikh, A. N.; Allara, D. L.; Azouz, I. B.; Rondelez, F. *J. Phys. Chem.* **1994**, *98*, 7577.
(21) Truong, K. D.; Rowntree, P. A. *J. Phys. Chem.* **1996**, *100*, 19917.
(22) Poirier, G. E.; Pylant, E. D. *Science* **1996**, *272*, 1145.
(23) Yamada, R.; Uosaki, K. *Langmuir* **1997**, *13*, 5218.
(24) Yamada, R.; Uosaki, K. *Langmuir* **1998**, *14*, 855.
(25) Xu, S.; CruchonDupeyrat, S. J. N.; Garno, J. C.; Liu, G. Y.; Jennings, G. K.; Yong, T. H.; Laibinis, P. E. *J. Chem. Phys.* **1998**, *108*, 5002.
(26) Tamada, K.; Hara, M.; Sasabe, H.; Knoll, W. *Langmuir* **1997**, *13*, 1558.
(27) Schreiber, F.; Eberhardt, A.; Schwartz, P.; Wetterer, S. M.; Lavrich, D. J.; Berman, L.; Fenter, P.; Eisenberger, P.; Scoles, G. *Phys. Rev. B* **1998**, *57*, 12476.
(28) Schwartz, P.; Schreiber, F.; Eisenberger, P.; Scoles, G. *Surf. Sci.* **1999**, *423*, 208.
(29) Eberhardt, A.; Fenter, P.; Eisenberger, P. *Surf. Sci.* **1998**, *397*, L285.

10.1021/ja0042783 CCC: $20.00
Published on Web 06/22/2001

anism to the latter has been observed at a characteristic temperature. It has been suggested that this temperature corresponds to the triple point on a quasiequilibrium 2D phase diagram,[5−7,16,20] and that monolayer growth corresponds to an isothermal path through this diagram.

In our previous studies of partial octadecylphosphonic acid (OPA) SAMs on mica, we have established, through comparisons of atomic force microscope (AFM) images, infrared (IR) spectra, and contact angle measurements, that this system (at room temperature) corresponds to the first class of growth mechanism described above;[13,17,30−32] i.e., a partial monolayer of OPA on mica consists of islands of approximately vertically oriented, close-packed, well-ordered molecules surrounded by essentially bare substrate (a 2D vapor phase of adsorbate molecules). To summarize the evidence, (1) atomic lattice AFM images were obtained of the mica surface in regions between islands,[30] (2) phase-contrast AFM images were consistent with a "hard" surface between islands, (3) the cosine of the contact angle of water or hexadecane extrapolated to near unity as the island coverage approached zero,[13,17,31,32] and (4) the methylene stretch peaks in the IR spectra were observed at positions corresponding to all-trans alkyl chains for fractional island coverages ranging from 0.1 to 1.[13] All of these observations were in distinct contrast with systems, such as octadecyltrimethylammonium bromide on mica[17] or OPA on sapphire at high temperatures,[16] where well-ordered molecular islands in partial films are believed to be surrounded by an intermediate density phase.

Although the *existence* of molecular islands during growth has been observed frequently, as discussed above, quantitative analysis has generally focused on the structural identification of various surface phases and the average surface coverage of these phases as a function of time. The evolution of the submonolayer film *morphology* (i.e. island nucleation and growth kinetics, island size distribution) has been addressed only rarely.[14,15] In our previous studies,[14,15] we found that nucleation and growth of submonolayer OPA islands could be described by a mechanism traditionally applied to vapor phase thin film growth (e.g. molecular beam epitaxy) at low temperatures. In a typical description of this mechanism, molecules impinge on the surface at rate F then undergo a 2D random walk with surface diffusion coefficient D, until they collide with each other, forming a stationary island, or with an existing island causing growth. In solution-phase deposition, F is proportional to the adsorbate concentration. A comprehensive kinetic investigation of SAM formation would involve the determination of kinetic parameters such as the rate of adsorption from solution, the surface diffusion coefficient, and the critical nucleus i. The critical nucleus is a fundamental concept in theories of nucleation and growth of thin films;[33−35] it corresponds to the number of molecules in the largest unstable island.

Many of the details of OPA island nucleation and growth[14,15] were described adequately by a kinetic rate equation approach under the point island approximation.[36−38] This approach leads to a description of thin film growth that includes four regimes: a low-coverage regime dominated by island nucleation, an intermediate coverage regime where nucleation slows and island growth becomes significant, an aggregation regime in which the island number density remains constant, and a coalescence regime. We were able to estimate the surface diffusion coefficient, critical nucleus, and deposition rate from measurements of surface coverage and island nucleation and growth in the intermediate growth regime.[14] A more robust calculation of the critical nucleus can be performed from the dependence of island density on deposition rate (i.e. concentration). Also, given the relatively high concentration of deposition solution used in our prior experiments, we were able to observe only the last three regimes (intermediate, aggregation, and coalescence) but not the predicted earliest regime of growth. The current experiments using lower concentrations allow us to observe the growth at very early stages and extend into the intermediate regime, overlapping the previous observations. In general, kinetic studies of island growth as a function of deposition rate allow a more complete understanding of SAM formation and permit a better comparison with theories of epitaxial growth kinetics than a study at a single deposition rate.

In this paper we report in situ atomic force microscope (AFM) observations of SAM growth using deposition solutions with concentrations in the range 0.01−0.45 mM (including previously reported data[14] obtained at a concentration of 0.17 mM). We find that the deposition rate from solution, i.e., number of molecules deposited per adsorption site per second, is directly related to the concentration. A longstanding prediction (by Venables[33]) relates the island number density to the deposition rate through the expression $N \sim F^{i/i+2}$. From measurements of the maximum island density at six different concentrations we directly test this predicted scaling and extract the size of the smallest stable submonolayer island.

Using the scaling of island density suggested by Venables (and scaling the time using relative concentrations) we demonstrate that island density data obtained at different concentrations can be collapsed onto a universal curve that explicitly shows all four regimes of growth: low coverage, intermediate coverage, aggregation, and coalescence. The same four regimes were reported in Monte Carlo simulations of vapor phase deposition of thin metallic and semiconductor films by molecular beam epitaxy (MBE).[36−38] The kinetics of island nucleation in the first two regimes are compared directly with these simulations and scaling predictions based on coupled rate equation approaches.

Experimental Details

AFM images were obtained with a Nanoscope III MMAFM (Digital Instruments, Santa Barbara, CA) in contact mode using silicon nitride cantilevers (spring constant approximately 0.12 (N/m)) and integral tips. The normal force (approximately 1 nN) exerted by the tip was continually minimized during imaging. To avoid surface contamination during in situ imaging the deposition solution came in contact with only glass, PTFE Teflon, and a fluoropolymer Kalrez O-ring (Dupont). Initially the fluid cell was filled with pure tetrahydrofuran (THF, 99.9%, Fisher Scientific) and images of the clean mica surface were collected. At time $t = 0$, solution (using THF as a solvent) containing approximately 0.01, 0.04, 0.08, 0.085, 0.17, or 0.45 mM octadecylphosphonic acid (OPA, $CH_3(CH_2)_{17}PO(OH)_2$) was allowed to flow into the fluid cell. The image acquisition was performed over a 2 μm × 2 μm area. At various stages during monolayer growth the scanned area was increased to 5 μm × 5 μm to verify that the smaller initial scanning area contained no signs of damage due to tip scanning. On some occasions, no monolayer growth whatsoever was observed; these experiments were abandoned under the assumption that the mica surface

(30) Woodward, J. T.; Ulman, A.; Schwartz, D. K. *Langmuir* **1996**, *12*, 3626.
(31) Woodward, J. T.; Gwin, H.; Schwartz, D. K. *Langmuir* **2000**, *16*, 2957.
(32) Woodward, J. T.; Schwartz, D. K. *Langmuir* **1997**, *13*, 6873.
(33) Venables, J. A. *Philos. Mag.* **1973a**, *27*, 697.
(34) Venables, J. A.; Spiller, G. D.; Hanbucken, M. *Rep. Prog. Phys.* **1984**, *47*, 399.
(35) Stoyanov, S.; Kashchiev, D. In *Current Topics in Materials Science*; Kaldis, E., Ed.; North-Holland: Amsterdam, 1981; Vol. 7, p 69.
(36) Amar, J. G.; Family, F.; Lam, P. M. *Phys. Rev. B* **1994**, *50*, 8781.
(37) Bartelt, M. C.; Evans, J. W. *Phys. Rev. B* **1992**, *46*, 12675.
(38) Tang, L. H. *J. Phys. I* **1993**, *3*, 935.

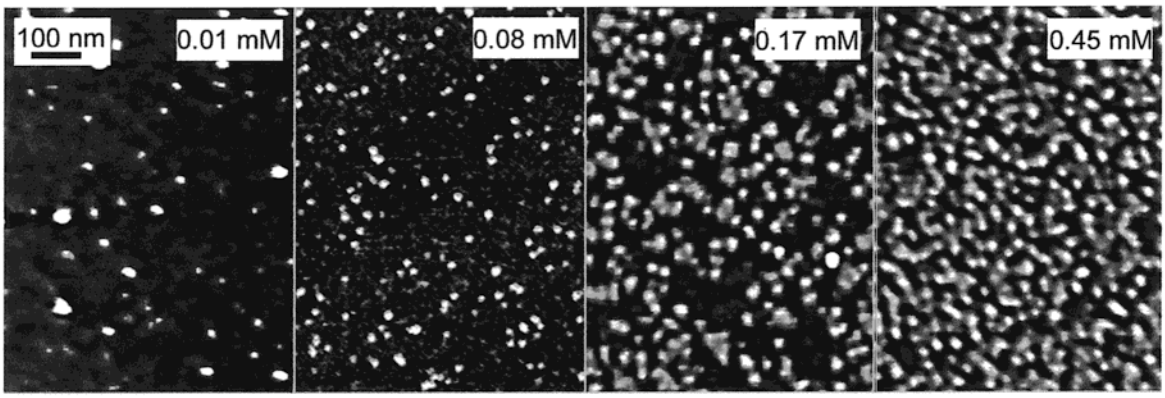

Figure 1. In situ AFM images (585 nm × 780 nm) showing the surface topology of an OPA monolayer at the stage of growth where the island density is at a maximum for four different concentrations of OPA molecules dissolved in THF. The annotation on each image represents the concentration of the deposition solution used to prepare the sample.

had somehow become contaminated. Image analysis was performed using NIH image software on images that were 2 μm × 2 μm in area. The island number density is reported in dimensionless units throughout, islands per adsorption "site", where the site area is taken to be the approximate cross-sectional area of an adsorbate molecule (0.25 nm^2).

Results and Analysis

Figure 1 shows four AFM images obtained in the stage of growth immediately prior to island coalescence, where the island number density is at its maximum value (N_{max}) for solutions containing 0.01, 0.08, 0.17, and 0.45 mM OPA dissolved in THF. The higher areas ("islands") are approximately 2 nm above the surrounding low areas (exceptions to this island height are discussed below), generally consistent with the molecular length of the adsorbate molecule. The magnitude of the height difference is consistent with the interpretation of islands composed of densely packed adsorbate molecules with the low areas being either bare substrate or a low-density phase (2D vapor) of adsorbate molecules. Earlier infrared spectroscopy and contact angle measurements on quenched partial OPA monolayers supported this picture.[13,17,30−32] One can clearly observe that an increase in solution concentration (and, hence, F) leads to a larger island number density.

Several qualitative features of the images are worthy of comment. The first image of the sequence captures a monolayer at a point where both surface coverage of the monolayer and island density are very low and tiny islands are frequently observed. At this stage, the height of the islands is apparently in the range 1.0−2.0 nm. This is somewhat shorter than one would expect from islands composed of fully extended (all-trans conformation) adsorbate molecules and also shorter than the typical island height observed for larger islands. This is true at later stages of growth as well; islands appear somewhat shorter when they first nucleate. We hypothesize that, even though the applied force during imaging is extremely low, these small islands are particularly easy to deform, and interaction with the AFM tip results in a tilt of the molecules in the islands. This is consistent with previous observations of thiol SAMs.[39] Nevertheless, careful comparison with regions surrounding the imaged area suggests that there is no significant wear due to imaging, nor is the growth affected significantly, provided the normal force exerted by the tip is maintained at the lowest values possible via continual adjustment.

The existence of islands displaying a range of heights presents an image analysis challenge, since very short islands may not be recognized in the island counting procedure (one must establish a height threshold to avoid counting noise or other artifacts as islands). The approach we have taken is to incorporate this issue into the experimental uncertainty by analyzing each image using a range of cutoff thresholds and determining the corresponding range of island numbers for each image. Thus, the error bars associated with island number density in this paper include both statistical uncertainty (using standard Poisson counting statistics) and uncertainty due to the image analysis procedure.

In the third and the fourth images of the sequence (Figure 1), when two or more islands are very close to each other, there often appears to be a gray halo "connecting" the islands. One possible explanation for this effect is a tip-size artifact due to the fact that a tip of finite dimensions cannot reach the substrate between the islands when the separation distance is too small. The fact that these features are more prominent with certain tips is also consistent with this explanation. In a few cases, however, these halos extend over distances larger than would be consistent with a tip size artifact (about 20 nm). We cannot offer a definitive explanation for these particular features; one possibility is that molecules near island edges are more easily deformed or tilted during scanning. In general, these artifacts do not significantly affect our ability to extract the *number* of islands in a given image, although they can introduce significant errors into measurements of island size or surface coverage (which are not discussed in the current paper).

One of the earliest and most robust predictions regarding epitaxial growth via islanding was Venables' relation between island density and deposition rate, $N \sim F^{i/i+2}$.[33] The same relation comes from more complex coupled rate equation approaches[36−38] and it has been verified by kinetic Monte Carlo simulations.[36−38,40,41] Although this may be applied, in principle, at several stages of growth, the most convenient way to consistently compare island densities of films grown at different deposition rates is to focus on the aggregation regime, where the island density is maximum, prior to the onset of coalescence. Figure 2 shows a log−log plot of the maximum island number density, N_{max}, as a function of the deposition solution concentration. The solid line represents the best fit to a power law dependence and yields an exponent of 0.30 ± 0.02. This value is consistent with an exponent of $^1/_3$, suggesting that $i = 1$, i.e., the smallest stable submonolayer island is composed of two molecules. A value of $i = 2$, for example, would predict an exponent of $^1/_2$, well outside the experimental uncertainties. The consistency of the island density values measured in experiments using 0.08 and 0.085 mM deposition solution respectively

(39) Barrena, E.; Kopta, S.; Ogletree, D. F.; Charych, D. H.; Salmeron, M. *Phys. Rev. Lett.* **1999**, *82*, 2880.

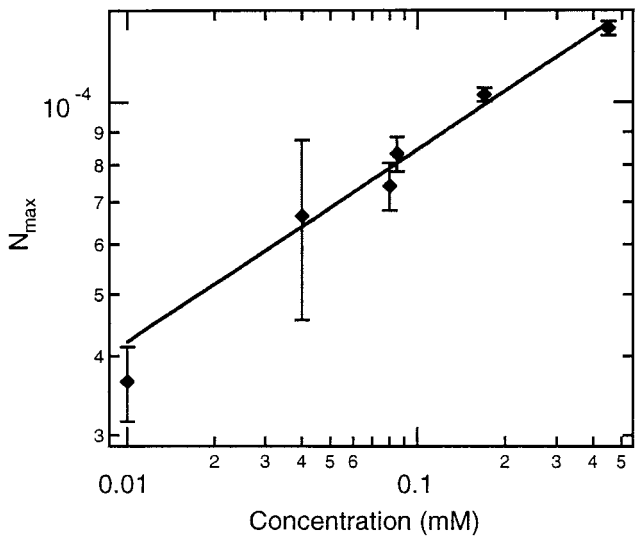

Figure 2. A log−log plot of the maximum island number density versus the concentration of the deposition solution. The line represents the best fit to a power law concentration dependence. The best fit exponent is 0.30 ± 0.02, consistent with a stable submonolayer island size of two molecules.

indicates the approximate degree of reproducibility we can expect in these experiments.

Due to the enormous dynamic range of exposure times necessary to observe all regimes of growth, we were not able to obtain a universal growth curve in a single experiment. However, using the concentration scaling suggested above, we can overlap data sets obtained at two different concentrations. Figure 3 shows a log−log plot of the scaled island density per molecular adsorption "site" as a function of the dimensionless time parameter *Ft*, where *F* is the deposition rate from solution in units of number of molecules deposited per "site" per second and *t* is the time in seconds. The plot summarizes data from experiments with two different solution concentrations, 0.01 (circles) and 0.17 mM (triangles). The higher concentration data was presented in a previous publication.[14] The absolute magnitude of *F* was extracted directly from observations of monolayer coverage vs time[14] for the higher concentration data set (0.17 mM), where the coverage measurements were more reliable. For the lower concentration experiment, the small size of the islands resulted in large uncertainties in monolayer coverage due to difficulty in deconvoluting the tip dimension from the island areas. Therefore, the relative scaling factor on the time axis was taken to be the ratio of the solution concentrations. The specific values of *F* used were 8.1×10^{-5} s^{-1} for the 0.17 mM data set and 4.6×10^{-6} s^{-1} for the 0.01 mM data. As suggested by the scaling with concentration shown in Figure 2 and discussed above, the island density is scaled by the factor $F^{-1/3}$, where, again, the relative values of *F* are taken from the ratio of the concentrations. Thus the *overlap* of the two data sets is based solely on the relative concentrations, suggesting that simple scaling theories provide an excellent description of the island nucleation kinetics.

Four regimes of growth were observed. In the low-coverage nucleation regime, the number of islands increased rapidly, indicating nucleation of new islands. The data in this regime are not consistent with a single power law exponent. In fact, there appears to be a crossover (at $Ft \approx 0.005$) between an exponent of ~2 (dashed line) and an exponent slightly greater than 3 (solid line). In the point island model,[36−38] the island density in this regime is predicted to go like $N \sim t^{i+2}$. This suggests that there are two possible nucleation mechanisms in this system, one where $i = 0$ and another where $i = 1$. A value of $i = 0$ corresponds to a unimolecular nucleation mechanism where individual molecules become immobilized (perhaps at isolated defect sites) and nucleate an island. Of course, such a unimolecular mechanism is expected to dominate at short times when the concentration of mobile adsorbate molecules is very small. As the adsorbate concentration grows and collisions become more likely, there is a crossover to the bimolecular ($i = 1$) nucleation mechanism. Figure 3 shows that the island density at the crossover time is less than 5% of the maximum value obtained in the aggregation regime. Therefore, we would not expect the unimolecular nucleation behavior at short times to have a significant effect on the maximum island density, as reflected in Figure 2, which is consistent with $i = 1$. The effect of the $i = 0$ nucleation mechanism can be observed only in the nucleation kinetics at very early times.

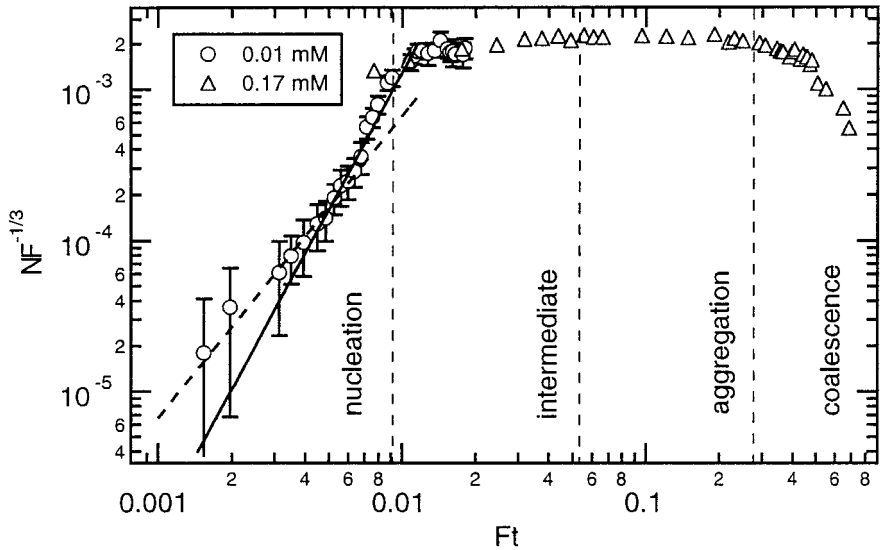

Figure 3. A log−log plot of the scaled island number density, $NF^{-1/3}$, versus *Ft*, where *F* is the deposition rate and *t* is the time. The scaling plot collapses two data sets with deposition solution concentrations of 0.01 (circles) and 0.17 mM (triangles), respectively. The dashed and solid lines drawn over the data in the nucleation regime represent power law exponents of 2 and 3, respectively.

In the intermediate coverage regime, the slope was reduced to a value of 0.31 ± 0.05, as we reported previously,[14] consistent with the point island (for $i = 1$) prediction of $^1/_3$.[36−38] In the aggregation regime the island density was nearly constant, the nucleation of new islands effectively ceased, and the molecules deposited from solution were consumed entirely by the growth of existing islands. In the coalescence regime the island density decreased due to processes where two or more islands merge with each other. The qualitative description of these four regimes as well as the specific power law nucleation kinetics in the low and intermediate coverage regimes are consistent with Monte Carlo simulations and kinetic rate law descriptions of epitaxial film growth.[33−38,40,41]

Figure 4 shows four sequences of representative AFM images, typical of the low-coverage nucleation regime (Figure 4a), intermediate-coverage regime (Figure 4b), aggregation regime (Figure 4c), and coalescence regime (Figure 4d), respectively. Each image is 300 nm × 600 nm in size and represents a small portion of a larger image: typically 2000 nm × 2000 nm. The island density values shown in Figure 3 were extracted from the full 2000 nm × 2000 nm images.[14] The images showing the low-coverage nucleation regime (Figure 4a) were acquired using approximately 0.01 mM OPA dissolved in THF. Those showing the later regimes (Figure 4b−d) were acquired using 0.17 mM OPA dissolved in THF.

In the low-coverage nucleation regime (Figure 4a), one can clearly observe nucleation events (indicated by white arrows), where an island appears in an area that was vacant in the previous image. To aid the eye, we have arbitrarily placed these arrows on the first image where a given island attains a height similar to the surrounding islands. As discussed above, in some cases the island may be visible, but shorter, in a preceding image. Growth of the existing islands in this low coverage regime is virtually undetectable. Nucleation of submonolayer islands is the dominant source of increase of the surface coverage in this regime, which is extremely low. Nucleation events are also observed in the intermediate regime (Figure 4b). In addition, existing islands gradually grow with time (indicated by black arrows). The total increase of submonolayer coverage in this regime is due to both nucleation of islands and island growth. In the aggregation regime (Figure 4c), nucleation of new islands has ceased (the island number density is constant as shown in Figure 3) and surfactant molecules adsorbed on the surface are consumed in the growth of the existing islands. Our previous analysis of the island size distribution in this regime showed that it was consistent with the concept of dynamical scaling, where a fundamental size distribution function is scaled by a single increasing length scale as coverage increases.[15] In the coalescence regime (Figure 4d), islands are observed to merge, reducing the island number density. Finally, the islands percolate across the sample and form continuous paths of monolayer traversing the image from side to side.

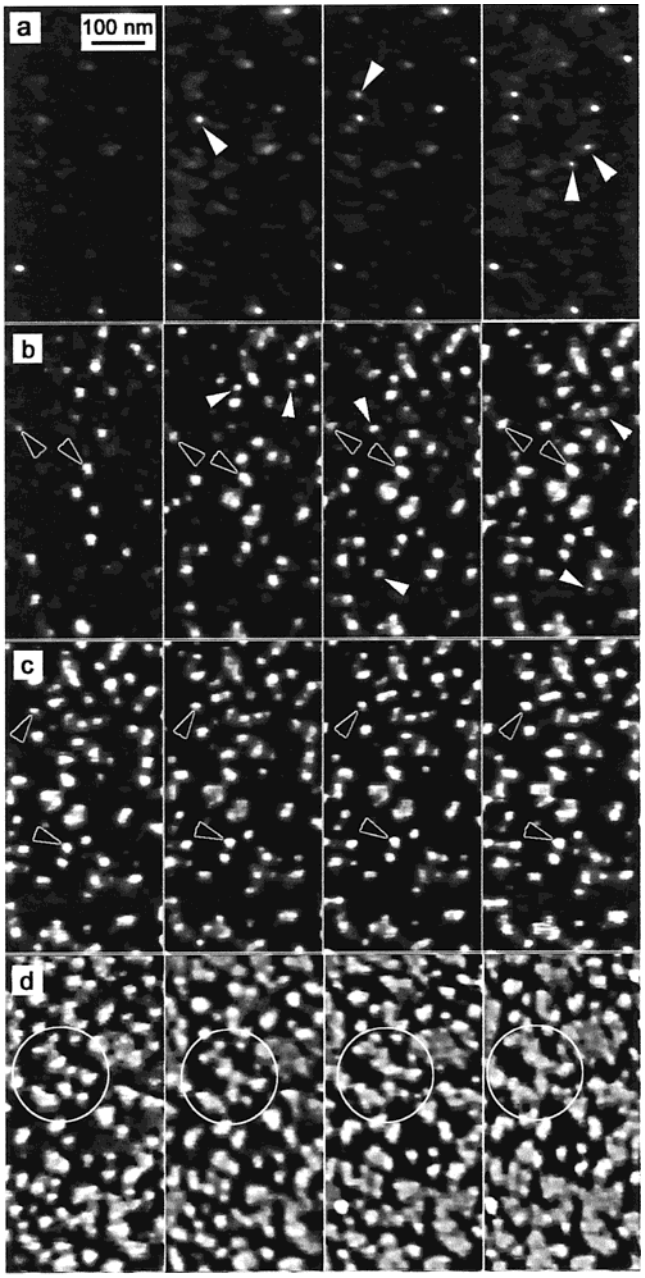

Figure 4. In situ AFM images (300 nm × 600 nm) showing the time evolution of the surface topology of OPA monolayers during the (a) low-coverage nucleation regime, (b) intermediate growth regime, (c) aggregation regime, and (d) coalescence regime. The images in each sequence show the same region of the monolayer during growth as time proceeds from left to right. The white arrows indicate examples of island nucleation while the black arrows indicate examples of island growth. The white circles in panel d indicate multiple coalescence events.

Discussion

Dynamic scaling theory and Smoluchowski-type rate equation approaches provide theoretical tools appropriate for describing island nucleation, aggregation, and coalescence processes during 2D cluster growth in a variety of systems. The acquisition of real time in situ AFM images during SAM growth allows application of these theoretical tools to solution-phase deposition of SAMs. We previously found that the kinetics of SAM growth could be described using the "point island" model of 2D cluster growth,[36−38] which postulates that the growth rate of islands is size-independent. This approximation is reasonable for widely separated islands where the 2D diffusion field is fully developed and vastly simplifies the system of coupled rate equations. This approach allowed us to calculate the surface diffusion coefficient, $D = 2.9(\pm 0.3) \times 10^{-9}$ cm^2/s, from the kinetics of island nucleation and from the growth kinetics of individual islands. In addition, from the overall coverage kinetics we were able to determine the deposition rate from solution, $F = 8.1(\pm 0.5) \times 10^{-5}$ s^{-1} (for 0.17 mM deposition solution).[14] The number and size distribution of submonolayer islands is sensitive to the ratio $R = D/F$.

In its simplest form, the point island model can be expressed as two coupled rate equations, one for the number density of isolated adsorbate molecules on the surface, N_1, and another for the total number of stable islands, N, containing $i + 1$ or more molecules

$$\frac{dN_1}{dt} = F - (i+1)DN_1^{i+1} - DNN_1$$

$$\frac{dN}{dt} = DN_1^{i+1}$$

where the terms on the right-hand side of the first equation represent deposition from solution, island nucleation, and island growth, respectively. An additional term for the loss of adsorbate molecules by desorption is neglected in the low-temperature approximation (the justification for this is discussed more fully below). Dividing both equations by F and introducing the dimensionless time $\theta = Ft$ and the dimensionless ratio $R = D/F$, we obtain

$$\frac{dN_1}{d\theta} = 1 - (i+1)RN_1^{i+1} - RNN_1$$

$$\frac{dN}{d\theta} = RN_1^{i+1}$$

Solving these coupled equations under approximations appropriate for the low coverage regime leads to the power law expression $N_{low} \sim R\theta^{i+2}$,[36] while approximations appropriate for the intermediate regime lead to $N_{int} \sim R^{-i/i+2}\theta^{1/i+2}$.[36-38] In the aggregation regime, the maximum island density is predicted to scale as $N_{agg} \sim R^{-i/i+2}$.[33-38] Our observations that $N_{low} \sim t^3$ (in the latter part of the low coverage regime), $N_{int} \sim t^{0.31}$, and $N_{agg} = N_{max} \sim F^{0.30} \sim R^{-0.30}$ confirm that this model provides a good description of island nucleation and growth in this SAM system. Furthermore, they are all consistent with the conclusion that $i = 1$, i.e., the smallest stable island consists of two molecules. The good overlap obtained by using these scaling relationships, between data sets obtained at concentrations differing by more than 1 order of magnitude, provides further evidence that the general picture behind this model is appropriate, as does the clear observation of each of the four expected regimes of growth.

Although the model presented above provides a fairly consistent description of the nucleation and growth kinetics, it is clearly simplistic in certain respects. For example, upon careful inspection of sequences such as those shown in Figure 3, one can find occasional examples of islands that temporarily decrease in size. This implies that molecules can detach from islands, a process unaccounted for in the particular model described. Furthermore, in other work[42,43] we explored the dissolution of OPA SAMs into very dilute solution and found clear evidence for molecular detachment from islands and desorption from the surface. There is every reason to believe that these processes occur to some extent during film *growth* as well. However, the agreement between the observed kinetic and predicted[33-38] power laws suggests that detachment and desorption do not play a major role in the island nucleation kinetics. For example, island nucleation and growth under conditions where desorption is significant (high temperatures), often called "incomplete condensation" in the literature, leads to a constant island nucleation rate ($N_{low} \sim t$), the maximum island density is predicted to scale as $N_{max} \sim F^i$, and no crossover from an early nucleation regime to an intermediate regime is predicted.[33,34] All of these predictions are incompatible with our observations. It is likely, however, that detachment and desorption will have a significant influence on film *morphology* (e.g., island size distribution and island shape).

Conclusions

The formation process of an octadecylphosphonic acid self-assembled monolayer deposited from solution onto mica was observed in real time at a variety of different concentrations using in situ atomic force microscopy. Four distinct regimes of growth were observed: (1) low coverage (nucleation), (2) intermediate, (3) aggregation, and (4) coalescence, consistent with theoretical models of epitaxial film growth at low temperatures. The maximum island number density had a power law dependence on solution concentration with an exponent of 0.30, consistent with the conclusion that the smallest stable submonolayer island is composed of two molecules ($i = 1$). The time dependence of the island density in the low coverage and intermediate regimes were also generally consistent with this value of the critical nucleus. At very early stages of the nucleation regime, there was evidence of a unimolecular ($i = 0$) nucleation mechanism. Island density data from experiments with different concentrations of deposition solution were collapsed onto a single universal growth curve using theoretical scaling relationships. These results present a comprehensive picture of SAM formation via an islanding mechanism that compares favorably with standard rate equation predictions of epitaxial film growth.

Acknowledgment. This work was supported by the National Science Foundation (grant No. CHE-9980250) and the Camille Dreyfus Teacher-Scholar Awards Program.

JA0042783

(40) Amar, J. G.; Family, F. *Phys. Rev. Lett.* **1995**, *74*, 2066.
(41) Amar, J. G.; Family, F. *Thin Solid Films* **1996**, *272*, 208.
(42) Doudevski, I.; Schwartz, D. K. *Langmuir* **2000**, *16*, 9381.
(43) Doudevski, I.; Schwartz, D. K. *J. Phys. Chem. B* **2000**, *104*, 9044.